Band gaps and leaky-wave effects in resonant photonic-crystal waveguides

Y. Ding and R. Magnusson

Department of Electrical and Computer Engineering, University of Connecticut, Storrs, CT 06269-2157
Robert.Magnusson@uconn.edu

Abstract: The paper addresses the leaky stop bands associated with resonant photonic crystal slabs and periodic waveguides. We apply a semianalytical model pertinent to the second band to compute the dispersion curves describing the leaky stop band and verify its correctness by rigorous band computations. This approximate model provides clear insights into the physical properties of the leaky stop band in terms of explicit analytical expressions found. In particular, it enables comparison of the structure of the bands computed in complex propagation constant, implying spatially decaying leaky modes, with the bands computed in complex frequency, implying temporally decaying modes. It is shown that coexisting Bragg-coupling and energy-leakage mechanisms perturb the bands in complex propagation constant whereas these mechanisms are decoupled in complex frequency. As a result, the bands in complex frequency are well defined exhibiting a clear gap. These conclusions are verified by numerical diffraction computations for both weak and strong grating modulations where the resonance peaks induced by external illumination are shown to closely track the band profile computed in complex frequency. Thus, in general, phase matching to a resonant leaky mode occurs via real propagation constant that is found by dispersion computations employing complex frequency.

©2007 Optical Society of America

OCIS codes: (050.0050) Diffraction and gratings; (050.1970) Diffractive optics; (310.0310) Thin films; (310.2790) Guided waves.

References and links

1. A. Yariv, *Optical Electronics in Modern Communications*, 5th edition (Oxford University Press, New York, 1997).
2. J. D. Joannopoulos, R. D. Meade, and J. N. Winn, *Photonic Crystals: Molding the Flow of Light* (Princeton, 1995).
3. K. Sakoda, *Optical Properties of Photonic Crystals* (Springer-Verlag, Berlin, 2001).
4. Y. Ding and R. Magnusson, "Resonant leaky-mode spectral-band engineering and device applications," Opt. Express **12,** 5661-5674 (2004).
5. D. Wawro, S. Tibuleac, R. Magnusson, and H. Liu, "Optical fiber endface biosensor based on resonances in dielectric waveguide gratings," Proceedings of the SPIE **3911**, 86-94 (2000).
6. B. T. Cunningham, B. Lin, J. Qiu, P. Li, J. Pepper, and B. Hugh, "A plastic colorimetric resonant optical biosensor for multiparallel detection of label-free biochemical interaction," Sens. Actuators B **85**, 219–226 (2002).
7. G. Purvinis, P. S. Priambodo, M. Pomerantz, M. Zhou, T. A. Maldonado, and R. Magnusson, "Second-harmonic generation in resonant waveguide gratings incorporating ionic self-assembled monolayer polymer films," Opt. Lett. **29**, 1108-1110 (2004).
8. Y. Ding and R. Magnusson, "Use of nondegenerate resonant leaky modes to fashion diverse optical spectra," Opt. Express **12**, 1885-1891 (2004).
9. R. F. Kazarinov and C. H. Henry, "Second-order distributed feedback lasers with mode selection provided by first-order radiation loss," IEEE J. Quantum Electron. **QE-21**, 144-150 (1985).
10. D. Rosenblatt, A. Sharon, and A. A. Friesem, "Resonant grating waveguide structures," IEEE J. Quantum Electron. **33**, 2038-2059 (1997).

#77691 - $15.00 USD Received 1 December 2006; revised 11 January 2007; accepted 12 January 2007

11. P. Vincent and M. Neviere, "Corrugated dielectric waveguides: A numerical study of the second-order stop bands," Appl. Phys. **20**, 345-351 (1979).
12. T. Tamir and S. Zhang, "Resonant scattering by multilayered dielectric gratings," J. Opt. Soc. Am. A **14**, 1607-1616 (1997).
13. D. L. Brundrett, E. N. Glytsis, T. K. Gaylord, and J. M. Bendickson, "Effects of modulation strength in guided-mode resonant subwavelength gratings at normal incidence," J. Opt. Soc. Am. A **17**, 1221-1230 (2000).
14. A. R. Cowan, P. Paddon, V. Pacradouni, and J. F. Young, "Resonant scattering and mode coupling in two-dimensional textured planar waveguides," J. Opt. Soc. Am. A. **18**, 1160-1170 (2001).
15. D. Gerace and L. C. Andreani, "Gap maps and intrinsic diffraction losses in one-dimensional photonic crystal slabs," Phys. Rev. E **69**, 056603 (2004).
16. T. K. Gaylord and M. G. Moharam, "Analysis and applications of optical diffraction by gratings," Proc. IEEE **73**, 894-937 (1985).
17. M. G. Moharam, E. B. Grann, D. A. Pommet, and T. K. Gaylord, "Formulation for stable and efficient implementation of the rigorous coupled-wave analysis of binary gratings," J. Opt. Soc. Am. A **12**, 1068-1086 (1995).
18. S. T. Peng, T. Tamir, and H. L. Bertoni, "Theory of periodic dielectric waveguide," IEEE Trans. Microwave Theory Tech. **MTT-23**, 123-133 (1975).
19. T. Tamir and S. Zhang, "Modal transmission-line theory of multilayered grating structures," J. of Lightwave Technol. **14**, 914-927 (1996).
20. D. L. Jaggard and C. Elachi, "Floquet and coupled-waves analysis of higher-order Bragg coupling in a periodic medium," J. Opt. Soc. Am. **66**, 674-682 (1976).
21. T. Tamir and S. T. Peng, "Analysis and design of grating couplers," Appl. Phys. **14**, 235-254 (1977).
22. C. Peng and W. Challener, "Input-grating couplers for narrow Gaussian beam: influence of groove depth," Opt. Express **12**, 6481-6490 (2004).

1. Introduction

Light propagation in periodic waveguides, diffractive elements, and photonic crystals is of practical interest in many areas of physics and engineering. Knowledge of the frequency stop bands associated with these structures is important in numerous applications as widely reported [1-3]. Consequently, the band structure of photonic lattices in one, two, and three dimensions has received considerable attention recently, in part motivated by improved ability to fabricate functional periodic elements with nanoscale feature control.

The objective of this paper is to formulate and explain the leaky stop bands characteristic of planar periodic waveguides, also referred to as waveguide gratings or photonic crystal slabs. These bands differ from the usual Bragg-type stop bands in that there exists an out-of-plane radiative energy-coupling channel; namely, the leaky mode resides above the light line in the first zone of the Brillouin diagram. An incident plane wave can induce a leaky waveguide mode on a waveguide-grating structure thereby generating a guided-mode resonance (GMR) field response in the spectrum. The resonance effect leads to the redistribution of diffracted energy and manifests as reflection and transmission peaks arising out of the background provided by the effective-medium thin-film characteristics of the structure. Nanophotonic devices operating under GMR conditions provide versatile functionalities and can be used for both narrowband and broadband filtering and polarization control [4]. Moreover, GMR elements may possess high Q factors and corresponding narrow linewidths thus being suitable for high sensitivity bio- and chemical sensors [5, 6]. The strong surface-localized electromagnetic fields associated with high-Q resonance also provide interesting means to study the nonlinear properties of biological and polymeric materials as well as for radiation generation in surface-localized active molecular species [7].

In recent papers, we discussed the application of leaky-mode resonance layers in photonic device design [4, 8]. Key to achieving functional devices with versatile spectral properties is placement and manipulation of the resonance peaks in the second stop band. Although not specifically addressing guided-mode resonance effects, the semi-analytical perturbation-theory formalism provided by Kazarinov and Henry [9] is well suited for explaining resonance behavior at the second band. Rosenblatt et al. applied the Kazarinov-Henry (KH) model in their studies of resonant grating behavior by including an external excitation wave as necessary for actual guided-mode resonance generation [10]. For gratings with symmetric

#77691 - $15.00 USD Received 1 December 2006; revised 11 January 2007; accepted 12 January 2007
(C) 2007 OSA

profiles, the KH model shows that the radiated fields generated by the two counterpropagating leaky modes can be in phase or out of phase at the edges of the second stop band. At one edge, there is zero phase difference and radiation is enhanced whereas at the other edge there is π phase difference quenching the radiation. In resonance elements with asymmetric profiles, there appears a resonance at each side of the second band gap [11, 8, 4]; for clarity, in this paper, we will only address the leaky-mode stop bands associated with symmetric profiles.

Vincent and Neviere presented dispersion curves for the second-order stop bands of periodic waveguides [11]. They showed results in real frequency k_0 versus complex propagation coefficient $\beta=\beta_R+j\beta_I$ that included the null in the imaginary part at the nonleaky edge. Noting that the k_0-β_R plot exhibited a forbidden gap that was not well defined, they turned to the complex frequency plane and demonstrated a clear band by numerical computations [11]. Leaky stop bands exhibiting distorted forbidden regions in k_0-β_R have since been reported in several papers [12, 13, 4]. In particular, large grating modulation has the effect of essentially obliterating the stop bands [4, 13] for the various supported leaky modes. In general, Brillouin diagrams computed in real frequency and complex propagation constant are valuable in analyzing resonance behavior in the various stop band regions. Use of complex frequency, however, results in clear stop bands [14, 15] as first observed by Vincent and Neviere [11]. One of the results of the present paper shows why the distortion of the real frequency bands occurs and why it does not occur in the complex frequency band.

In this paper, we compute dispersion curves for one-dimensional single-layer periodic waveguides. We are particularly interested in the dispersion behavior around the second stop band. Results generated with a semi-analytical coupled-mode model [9, 10] are verified with rigorous computations. Shown in Fig. 1 is the model periodic waveguide, or photonic crystal slab, sandwiched by a cover region and a substrate. Because the effective refractive index of the periodic layer is higher than the cover and substrate indices, it can function as a guiding layer. The grating has binary modulation and the modulation profile can, in principle, be either symmetric or asymmetric [8]; however, only the symmetric profile as presented in Fig. 1 will be treated in this paper. The structures under study will have differing high and low refractive indices (n_h and n_l); here, the effective index of the guiding layer (n_{avg}) is kept constant to highlight the effect of changes in modulation level. We use a parameter $\Delta\varepsilon=n_h^2-n_l^2$ to represent the level of modulation. The diffraction problem is solved using a rigorous coupled-wave analysis (RCWA) formulation [16, 17] whereas rigorous dispersion results are computed with the method introduced by Peng et al. [18] and Tamir et al. [19]. The frequency and propagation constant are presented in normalized form as k_0/K (=ωΛ/2πc where ω is the frequency and c is the speed of light in vacuum) and β/K, respectively, with $K=2\pi/\Lambda$ and Λ being the grating period. We assume that between k_0/K and β/K, one quantity is complex and the other real. Which one of these is complex is implied by the usage of subscripts *R* and/or *I*.

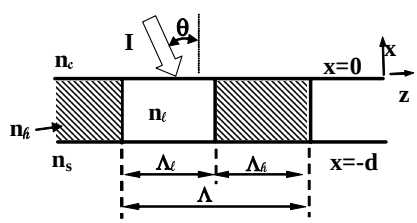

Fig. 1. The periodic waveguide under study. Thickness d=0.5μm, period Λ=1μm, fill factor $F=\Lambda_h/\Lambda$=0.4, cover region index n_c=1.0, substrate index n_s=1.5, n_{avg}=2, and $n_{avg}=\sqrt{Fn_h^2+(1-F)n_l^2}$. θ is the angle of incidence. The incident wave is in the TE polarization state such that the electric vector is normal to the plane of incidence.

#77691 - $15.00 USD Received 1 December 2006; revised 11 January 2007; accepted 12 January 2007
(C) 2007 OSA

2. Dispersion characteristics of periodic waveguides

Dispersion plots for a periodic waveguide are shown in Fig. 2 for the fundamental *TE* mode (TE_0). Figure 2(a) shows the first Brillouin zone where we display the first three stop bands. The solid line denotes the leaky mode and the dashed curves provide the light lines corresponding to the substrate (k_0n_s/K) and cover (k_0n_c/K). At a particular frequency beyond the first stop band, a leaky wave with $\beta_I \neq 0$ appears as shown in Fig. 2(b). When the frequency increases, a new leaky wave emerges and radiates into the cover or substrate when the Rayleigh conditions, expressed in the first zone,

$$k_0n_c - mK = -Re(\beta) \quad \text{or} \quad k_0n_s - mK = -Re(\beta) \tag{1}$$

are satisfied. There, k_0 is the wave number in free space, m is the index of the diffracted order, $K=2\pi/\Lambda$, and β is the propagation constant. These conditions are satisfied at the intersections of the folded light lines (dashed lines) and the β_R curve (solid line) as shown in Fig. 2(a).

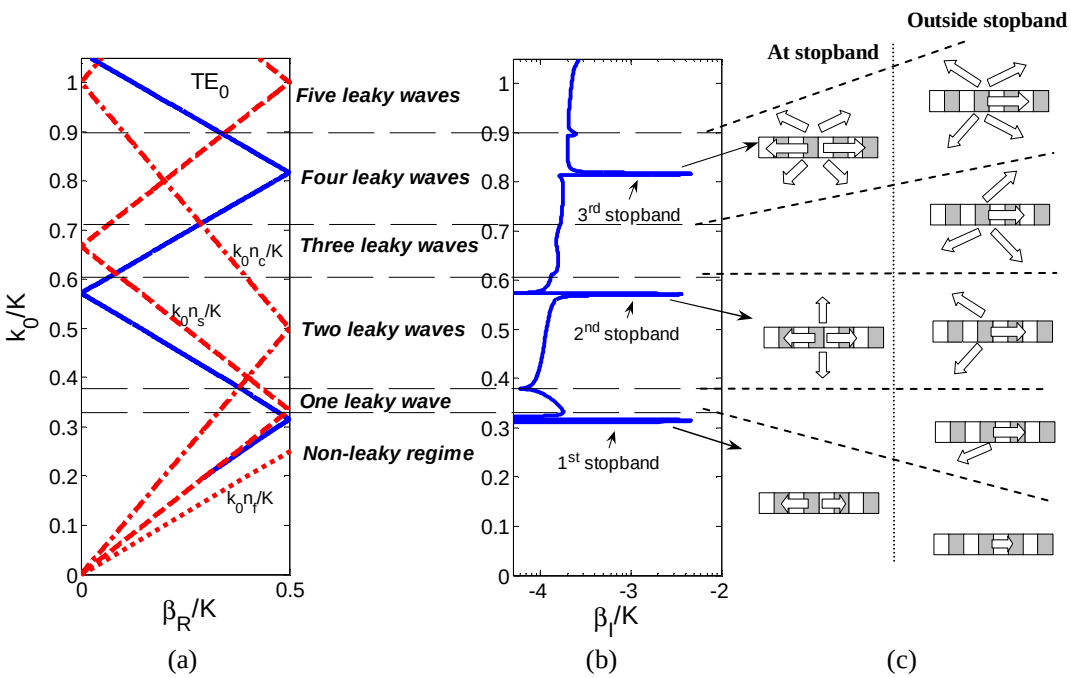

Fig. 2. Dispersion diagram for the TE_0 mode in a periodic waveguide. The propagation constant of the leaky mode is separated into real part and imaginary part with $\beta=\beta_R+j\beta_I$. (a) Real part of the propagation constant. (b) Imaginary part of the propagation constant; β_I is presented on a logarithmic scale. (c) Schematics showing the directions of modes and excited waves in and outside of the stop bands. The plot in (a) is reduced to the first Brillouin zone and only half of that zone is presented. The structure is that in Fig. 1 with n_h=2.05, $\Delta\varepsilon$=0.34, and $n_f = n_{avg}$.

Based on the Rayleigh points of Eq. (1), the dispersion diagram can be separated into regimes. In the non-leaky regime, the periodic waveguide supports purely bounded modes and no waves leak into the cover or substrate. As the refractive index of the substrate is higher than that of the cover in this example, the folded light line of the substrate intersects the dispersion curve at the first Rayleigh point. Starting from this point, which is beyond the first stop band, a radiation wave leaks into the substrate as illustrated in Fig. 2(c). The purely bounded mode thereby changes into a leaky mode and the propagation constant becomes complex as indicted in Fig. 2(b). Subsequently, the second Rayleigh point will be reached and a radiation wave also leaks into the cover. Additional waves emerge from the grazing angle as the frequency increases. The appearance of a new leaky wave may generate a perturbation on the β_I curve as shown in Fig. 2(b).

#77691 - $15.00 USD Received 1 December 2006; revised 11 January 2007; accepted 12 January 2007
(C) 2007 OSA

The stop bands form at the Bragg condition $\beta_R=qK/2$, where q is an integer denoting the band. The stop band can be identified by its significantly high value of β_I as shown in Fig. 2(b). As the figure shows, the coupling of two counter-propagating waveguide modes within a band is generally considerably stronger than the coupling between the waveguide mode and the radiating wave at moderate modulation levels. In the present example, the first stop band (q=1) occurs around normalized frequency k_0/K=0.315; the second stop band (q=2) is near frequency 0.571; and the third stop band (q=3) is at frequency 0.816. Details of these stop bands are presented in Fig. 3. As the first band is located in the non-leaky regime, it is a non-leaky stop band. Higher bands, such as the second and third stop bands, are thus leaky stop bands. In the first stop band, β_R is a constant across the band.

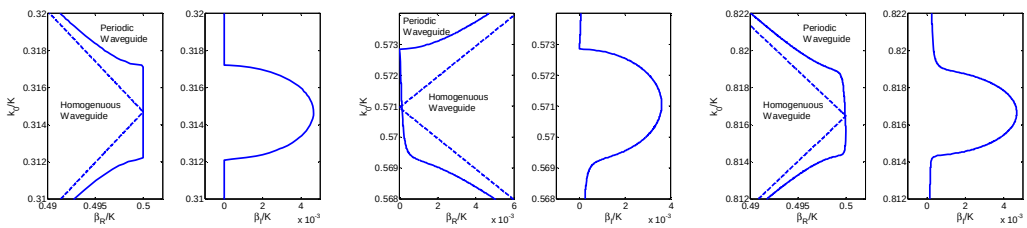

(a) (b) (c)

Fig. 3. Stop band details. (a) The first stop band. (b) The second stop band. (c) The third stop band. The dashed curves show the corresponding homogeneous waveguide dispersion valid for $\Delta\varepsilon$ approaching zero.

Dispersion plots can be presented in two different ways. One approach uses real frequency and complex propagation constant as in Figs. 2 and 3. The second method employs complex frequency and real propagation constant. Even though both are solutions to the same homogeneous system of equations, the two sets of dispersion results offer different, albeit complementary, perspectives on the leaky mode. In the first type of representation, the imaginary part of the propagation constant accounts for spatial attenuation. As the mode propagates along the periodic waveguide, its amplitude decays due to Bragg reflection and energy leakage by radiation. In the second type of representation, the imaginary part of the frequency defines a temporal decay rate. The difference between these points of view will be clarified with the coupled-mode model.

3. Second-band coupled-mode model

For small modulation $\Delta\varepsilon$, the dispersion properties at the second stop band can be approximated as [9]

$$\Delta\beta^2=\left[\left(\Delta k\cdot h_3\right)^2-\left|h_2\right|^2\right]+2jh_1\left[\left(\Delta k\cdot h_3\right)-\mathrm{Re}\left(h_2\right)\right] \tag{2}$$

or, expressed in a different form, as

$$\left(\Delta k\cdot h_3+jh_1\right)^2=\Delta\beta^2+\left(\left|h_2\right|^2+2jh_1\,\mathrm{Re}\left(h_2\right)-h_1^2\right) \tag{3}$$

where $\Delta\beta$ is the deviation from the Bragg condition ($\Delta\beta=\beta-K$) at the second stop band and Δk is the deviation of the wave number from the stop band center k_{center} whence $\Delta k=k_0-k_{center}$. As presented in Fig. 4, the coefficient h_1 represents the coupling between a guided wave and a leaked wave. This coupling is first-order coupling that is assisted by the grating vector $\vec{K}$. The coefficient h_2 represents the second-order coupling between the two counter-propagating waveguide modes and h_3 is a coefficient related to the group velocity of the unperturbed waveguide mode and can be treated as a group index [9, 10]. Note that $\Delta\beta=\Delta k h_3$ when there is no modulation (homogenous waveguide). We refer to this theoretical approach as the Kazarinov-Henry (KH) coupled-mode model.

#77691 - $15.00 USD Received 1 December 2006; revised 11 January 2007; accepted 12 January 2007
(C) 2007 OSA

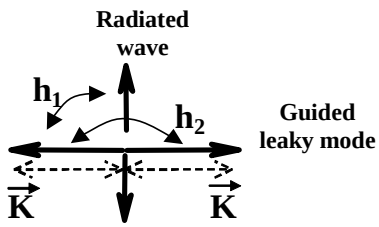

Fig. 4. Coupling processes at the second stop band.

For the model in Fig. 1, the coupling coefficients h_1, h_2 and h_3 are given by [9]

$$\text{TE mode}\begin{cases} h_1 = \dfrac{jk_0^4\gamma_1^2}{2K}\int_{-d}^{0}\int_{-d}^{0}\phi(x')\phi^*(x)G(x,x')\,dx'dx \\ h_2 = \dfrac{k_0^2\gamma_2}{2K}\int_{-d}^{0}\phi(x)\phi^*(x)\,dx \\ h_3 = \dfrac{k_0}{K}\int_{-\infty}^{\infty}\gamma_0(x)\phi(x)\phi^*(x)dx \end{cases} \tag{4}$$

where γ_0, γ_1 and γ_2 are the 0th, 1st and 2nd Fourier coefficients of the relative permittivity modulation profile, respectively. For a binary profile, γ_0, γ_1 and γ_2 are constant throughout (i. e. not x-dependent) the grating layer. $G(x,x')$ is the Green's function for the diffracted field [10] and $\phi(x)$ denotes the mode profile. All the coefficients are wavelength/frequency dependent. However, in this paper, for convenience, the coefficients used in the coupled mode model are assumed to be wavelength independent with numerical values evaluated at normalized frequency 0.571, the second band center (estimated from the dispersion properties of the equivalent homogenous waveguide). Under this treatment, h_3 is constant, while h_1 and h_2 are proportional to $\Delta\varepsilon^2$ and $\Delta\varepsilon$, respectively. These assumptions are appropriate for small modulation with the frequency under consideration varying across a limited range. At high modulation, these assumptions do not work well because of two factors. First, the stop-band width generally expands as modulation increases. Second, the band may shift when higher-order coupling becomes significant [20]. Nevertheless, as shown in the paper, the KH model, as expressed in the form of Eqs. (2) and (3), can provide valuable information even under relatively strong modulation.

4. Physical properties of the leaky stop band

By forcing either frequency or propagation constant to be real, two sets of dispersion results can be obtained from the coupled-mode approach expressed by Eqs. (2) and (3). One set applies real frequency and complex propagation constant; the other uses real propagation constant and complex frequency. We will first discuss the versions of Eqs. (2) and (3) relevant to the nonleaky stop band. In this case, h_1=0 and Eqs. (2) and (3) become

$$\Delta\beta = \pm\sqrt{(\Delta k\cdot h_3)^2 - |h_2|^2} \tag{5}$$

and

$$\Delta k = \pm\sqrt{(\Delta\beta)^2 + |h_2|^2}\Big/h_3 \tag{6}$$

It is noted that Eq. (5) is similar to Eq. (13.5-6) in [1].

Equation (5) can be used to generate dispersion curves with real frequency. As shown in Fig. 5(a), the propagation constant has an imaginary part for a range of frequencies satisfying $|\Delta k h_3|<|h_2|$. Figure 5(b) is computed with Eq. (6) presenting the dispersion characteristics with

#77691 - $15.00 USD Received 1 December 2006; revised 11 January 2007; accepted 12 January 2007
(C) 2007 OSA

real propagation constant; note that there exists no solution for frequencies Re($\Delta k h_3$)<$|h_2|$. Outside the bands in Fig. 5, the imaginary part of either propagation constant or frequency is zero as there is no radiation leakage in this case. In addition, the real parts of the curves in Figs. 5(a) and 5(b) are exactly the same.

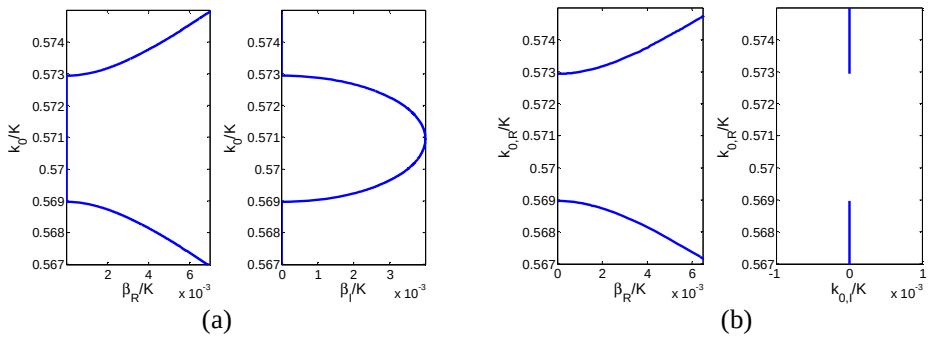

Fig. 5. Details of a nonleaky stop band. (a) Dispersion represented with real frequency and complex propagation constant. (b) Dispersion represented with complex frequency and real propagation constant. The complex frequency is defined by $k_0=k_{0,R}+jk_{0,I}$. Only half of the first Brillouin zone is plotted. The plots are calculated for the structure in Fig. 1 (n_h=2.05) while forcing the coupling coefficient h_1 to zero.

4.1. Band structure in complex propagation constant

Figure 6 presents leaky-band dispersion results computed with real frequency and complex propagation constant. In this case, the real part of the propagation constant is not constant in the band and the imaginary part is nonzero both inside and outside the band. As illustrated in Fig. 2, outside the band, the imaginary part originates in energy leaked into the substrate and cover. Inside the band, both leaked energy and Bragg coupling contribute to the imaginary part of the propagation constant. In this example with modulation $\Delta\varepsilon$=0.34, the results obtained from Eqs. (2) or (3) agree with rigorous computations verifying that the coupled-mode model holds well around the leaky band.

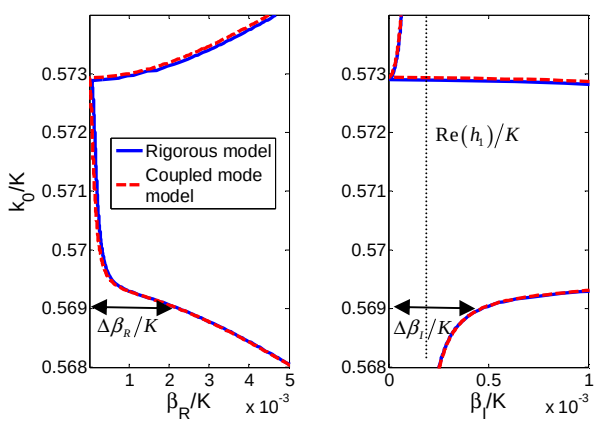

Fig. 6. Details of a leaky stop band at small modulation (n_h=2.05 and $\Delta\varepsilon$=0.34). The dispersion curves are formulated in real frequency and complex propagation constant.

For additional insights, we examine special points in frequency. At frequency $\Delta k = h_2/h_3$, we get $\Delta\beta = 0$ from Eq. 2, which defines the upper band edge in Fig. 6. At this edge, h_1 has no effect on the propagation constant as β_I = 0 and the wave appears nonleaky. The lower edge is not as obvious. If we use the criterion that the band edge should appear at minimum

#77691 - $15.00 USD Received 1 December 2006; revised 11 January 2007; accepted 12 January 2007
(C) 2007 OSA

$\partial k/\partial\beta_R$ (which is analogous to group velocity), it can be shown that the lower edge locates at approximately $\Delta k = -h_2/h_3$ in the case of small modulation. At this edge, by Eq. (2), we have $\Delta\beta = \Delta\beta_R + j\Delta\beta_I = \sqrt{-4jh_2h_1}$ (note that h_1 is generally a complex number as indicated in Eq. 4). Thus, both the real and imaginary parts of the propagation constant are nonzero and proportional to both h_1 and h_2. At frequencies far from the band edges with $|\Delta k| >> h_2/h_3$, one has $\Delta\beta \approx \sqrt{(\Delta k h_3)^2 - h_2^2} + jh_1$. Therefore, the imaginary part of the propagation constant converges to Re(h_1) away from the band as shown in Fig. 6. This indicates that the real part of h_1 represents the actual amount of energy leaked out of the waveguide as discussed by Rosenblatt et al. [10].

4.2. Band structure in complex frequency

Figure 7 presents the dispersion characteristics of the same leaky band using a real propagation constant. Unlike the previous rendition in Fig. 6, an unambiguous stop band is observed. Outside the band, the frequency has an imaginary part. Again, the characteristics of the stop band are well captured by the KH coupled-mode model with simplified analytical expressions available in special cases. At $\Delta\beta = 0$, the model gives two solutions $\Delta k = h_2/h_3$ and $\Delta k = -(h_2 + 2jh_1)/h_3$. The former represents the upper band edge as shown in Fig. 7. At this edge, Δk is real agreeing with the results from analysis obtained with real frequency; since $k_{0,I}$=0, no leakage occurs. The latter expression represents the lower band edge as shown in the figure where Δk has an imaginary part equal to $-2\mathrm{Re}(h_1)/h_3$ inducing energy leakage. At frequencies far from the band edges, one has $\Delta k = (\pm\Delta\beta - jh_1)/h_3$ with the imaginary part of Δk converging to $-\mathrm{Re}(h_1)/h_3$ as shown in Fig. 7.

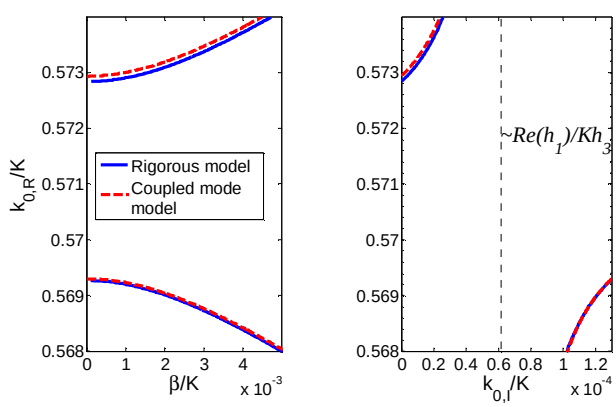

Fig. 7. Details of a leaky stop band at small modulation (n_h=2.05 and $\Delta\varepsilon$=0.34). The dispersion curves are formulated in complex frequency and real propagation constant.

4.3 Summary of analytical results

These results are summarized in Table I. At the nonleaky edge, the two representations give the same results. Away from the band, the results are comparable since $\Delta\beta=\Delta k h_3$. In the stop band and at the leaky edge, the results in real and complex frequency differ significantly in their relations to the coexisting coupling mechanisms (Bragg coupling and leaky wave coupling). For example, the representation with complex β keeps track of the spatial decay associated with each mechanism whereas the representation in complex k lumps the effects of these mechanisms together with the mode decay represented as temporal decay or radiation lifetime given by $Im(k)^{-1}$. In particular, as seen in the table, both $\Delta\beta_R$ and $\Delta\beta_I$ in the band

#77691 - $15.00 USD Received 1 December 2006; revised 11 January 2007; accepted 12 January 2007
(C) 2007 OSA

center and at the lower (leaky) edge, depend on both coefficients h_1 (leak) and h_2 (Bragg). In contrast, for complex k, Δk_R at the lower edge depends only on h_2 whereas Δk_I depends only on h_1. Thus, for the band in complex frequency, the two mechanisms are decoupled accounting for the well-defined band gap observed. Moreover, there are no solutions found in the band center consistent with no states existing there. Figure 8 shows a comparison of the band structure for these two cases computed with RCWA.

Table I. Main features of leaky stop bands in real and complex frequency

		Complex $\beta = \beta_R + j\beta_I$, real Δk	Complex $k = k_R + jk_I$, real $\Delta\beta$
Bandedge#1 (upper edge in the example treated)	$\Delta\beta_R$	0	0
	$\Delta\beta_I$	0	
	Δk_R	h_2/h_3	h_2/h_3
	Δk_I		0
Band center	$\Delta\beta_R$	$\mathrm{Re}\left(\sqrt{-h_2^2 - 2jh_2h_1}\right)$	0
	$\Delta\beta_I$	$\mathrm{Im}\left(\sqrt{-h_2^2 - 2jh_2h_1}\right)$	
	Δk_R	0	No solution
	Δk_I		No solution
Bandedge#2 (lower edge in the example treated)	$\Delta\beta_R$	$\mathrm{Re}\left(\sqrt{-4jh_2h_1}\right)$	0
	$\Delta\beta_I$	$\mathrm{Im}\left(\sqrt{-4jh_2h_1}\right)$	
	Δk_R	$-h_2/h_3$	$-h_2/h_3$
	Δk_I		$-2\,\mathrm{Re}(h_1)/h_3$
Away from band	$\Delta\beta_R$	$\sqrt{(\Delta k h_3)^2 - h_2^2}$	$\neq 0$
	$\Delta\beta_I$	$\mathrm{Re}(h_1)$	
	Δk_R	$\neq 0$	$\pm\sqrt{\Delta\beta^2 + h_2^2}/h_3$
	Δk_I		$-\mathrm{Re}(h_1)/h_3$

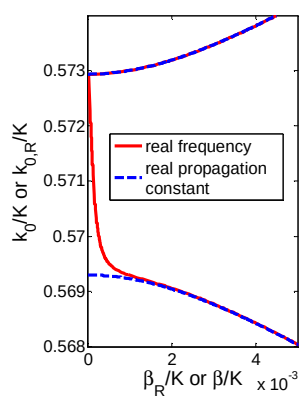

Fig. 8. Rigorously computed leaky stop band structure in real and complex frequency confirming the predictions of the KH model in Figs. 6 and 7 and in Table I.

#77691 - $15.00 USD Received 1 December 2006; revised 11 January 2007; accepted 12 January 2007
(C) 2007 OSA

The location of the nonleaky bandedge relates to the sign of h_2. For the example structure treated (Fig. 1) whose results are presented in Figs. 6-8, the coefficient h_2 is real and positive since the modulation profile is symmetric. The fill factor F<0.5 and thus $\Delta\beta$ is zero at the upper edge in this particular example [13, 8]. Both the real and imaginary parts of $\Delta\beta$ are proportional to $\Delta\varepsilon^{1.5}$ since $h_1 \propto \Delta\varepsilon^2$ and $h_2 \propto \Delta\varepsilon$. Again, the difference between the real parts of β in the two representations originates in the leakage of the energy from the waveguide grating. At moderate modulation, the real parts of the two sets converge quickly when the frequency is away from the band as shown in Fig. 8.

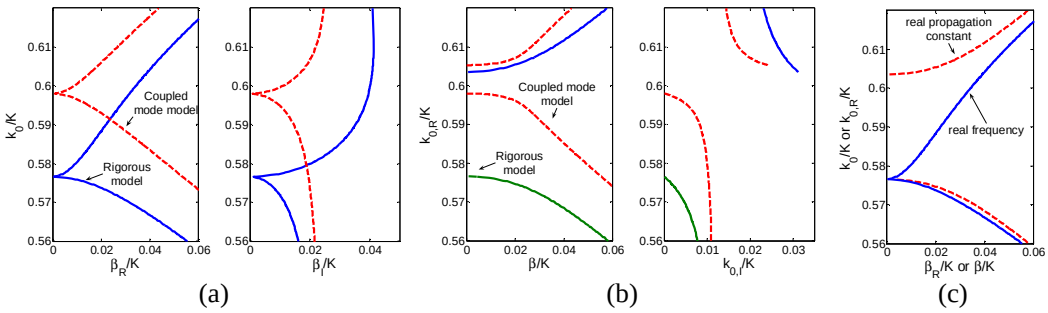

Fig. 9. Details of a leaky stop band with strong modulation (n_h=2.6 and $\Delta\varepsilon$=4.6) computed with the KH coupled-mode formalism and with RCWA. (a) Dispersion represented with real frequency and complex propagation constant. (b) Dispersion represented with complex frequency and real propagation constant. (c) Comparison of the real parts of β using RCWA.

4.4 Extension to strong modulation

Because the leakage of the energy is defined by $h_1 \propto \Delta\varepsilon^2$, the difference between the real and complex frequency dispersion formulations will be amplified under strong modulation. This is illustrated in Fig. 9. From Figs. 9(a) and 9(b), we see that the dispersion plots in real frequency do not give a clearly defined band gap while the set in complex frequency does. The KH model provides qualitatively correct results even for this high level of grating modulation. Again, both representations obtain the same nonleaky edge located at approximately k_0/K=0.577 for this example. It is interesting to note that the nonleaky edge has shifted to the lower side of the band (compare with Figs. 6 and 7). This will be explained in a future publication; we can show that the transition point is at $h_2=Re(h_1)$.

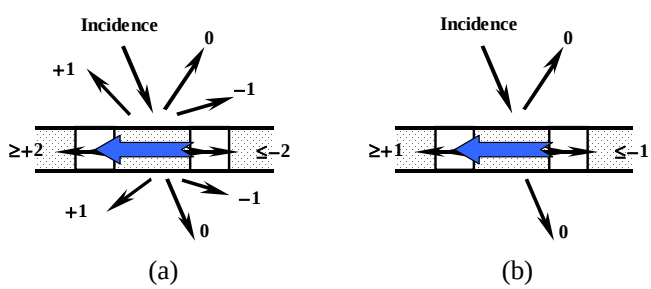

Fig. 10. Interaction between a periodic waveguide and an incident plane wave. (a) Excitation of a leaky mode in a higher-order diffraction regime. (b) Excitation of a leaky mode in the zero-order diffraction regime.

5. Guided-mode resonance excitation on periodic waveguides

Thus far, we have treated the leaky-mode resonance eigenvalue problem obtaining the dispersion properties pertaining to periodic waveguides or photonic crystal slabs. Since we are additionally interested in comparing these results with diffraction efficiency maps in the ω-β plane, we turn our attention to the resonance response of these elements on excitation with

#77691 - $15.00 USD Received 1 December 2006; revised 11 January 2007; accepted 12 January 2007
(C) 2007 OSA

external illumination. Figures 10(a) and 10(b) show resonance interactions between the periodic waveguide and an incident plane wave. At short wavelength (high frequency), as the grating has low spatial frequency with respect to the incident wave, there exist propagating orders other than the zero orders. As the wavelength increases, the propagation angles of the higher-order waves increase. Eventually, all the higher-order waves will become evanescent, or cut off, and the zero-order regime prevails. In multi-wave and in zero-order regimes, the higher-order evanescent waves can induce a resonance by coupling to a leaky mode as illustrated in Figs. 10(a) and 10(b). Because of the involvement of a waveguide mode, the physical picture associated with the resonance is clearly communicated by the term "guided-mode resonance." Since the resonance involves a particular diffraction order coupled to a particular mode, we label the GMRs as $TE_{m,v}$; for example, $TE_{2,1}$ is the resonance formed by the coupling between the second diffracted order and the TE_1 mode.

The GMRs manifest as rapid spectral variations of the diffraction efficiencies of the propagating waves. In Fig. 11, GMRs $TE_{1,0}$, $TE_{2,0}$ and $TE_{2,1}$ can be observed at normalized frequencies (k_0/K) 0.57, 1.06 and 1.23 respectively. Because GMR $TE_{1,0}$ resides in the zero-order diffraction regime, there is no energy lost to propagating higher-order diffracted waves and the resonance peak has 100% reflectance theoretically. The higher-order diffraction regime begins approximately at frequency 0.67, at which the ±1 diffraction orders emerge from the waveguide as propagating waves on the substrate side. Additional propagating orders will appear as the frequency increases.

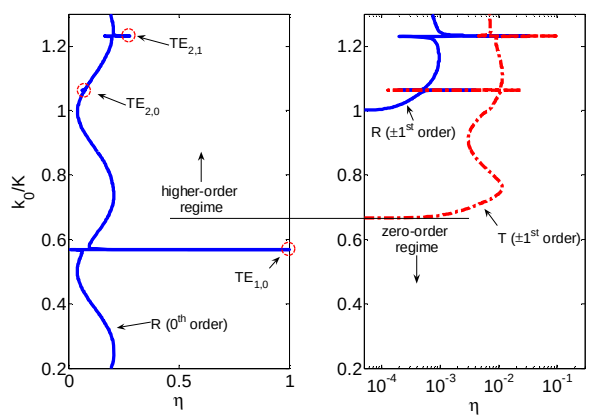

Fig. 11. Spectra of a single-layer waveguide grating under normal incidence θ=0°. The GMRs are marked by small circles. Here, η denotes diffraction efficiency, R reflectance, and T transmittance. The structure is that in Fig. 1 with n_h=2.05 and $\Delta\varepsilon$=0.34 with corresponding dispersion diagram shown in Fig. 2.

We remark that these computed results are obtained assuming plane-wave incidence. Thus, in this paper, we do not address effects associated with the coupling of optical beams with finite transverse cross section and the attendant non-planar phase fronts. For discussion of grating coupling involving finite beams, we refer the reader to references [21, 22].

6. Association of dispersion and resonance

The resonance effects induced on photonic-crystal waveguides are closely related to their dispersion properties. Specifically, the locations of the GMRs and Rayleigh transition points can be found from the dispersion plots as discussed above. For an obliquely incident excitation wave, as shown in Figs. 12(a) and 12(b), GMRs appear when the dispersion curve of the incident wave ($k_0 n_c \sin\theta$) crosses the β_R curve because the cross point is a solution of the phase matching condition. Note that these GMRs are not near any of the stop bands. The graph reveals the order-mode pair contributing to the resonance; for example, $TE_{+2,0}$ is identified as the corresponding cross point on the β_R curve of the TE_0 mode that is folded backwards twice. A new diffracted order emerges when the dispersion curve of the incident

#77691 - $15.00 USD Received 1 December 2006; revised 11 January 2007; accepted 12 January 2007
(C) 2007 OSA

wave intersects the folded light lines seen by comparing Figs. 12(a) and 12(c). Thus the higher diffraction orders whose diffraction efficiency η is plotted in Fig 12(c) emerge when

$$k_0 n_c \sin\theta - mK = \pm k_0 n_c \text{ or } k_0 n_c \sin\theta - mK = \pm k_0 n_s \tag{7}$$

is satisfied. In Eq. (7), a minus sign is used when the dispersion curve is folded odd number of times while the positive sign corresponds to even number of foldings. In Fig. 10(b), it is seen that the resonance efficiency can be substantially high even in a multiwave regime.

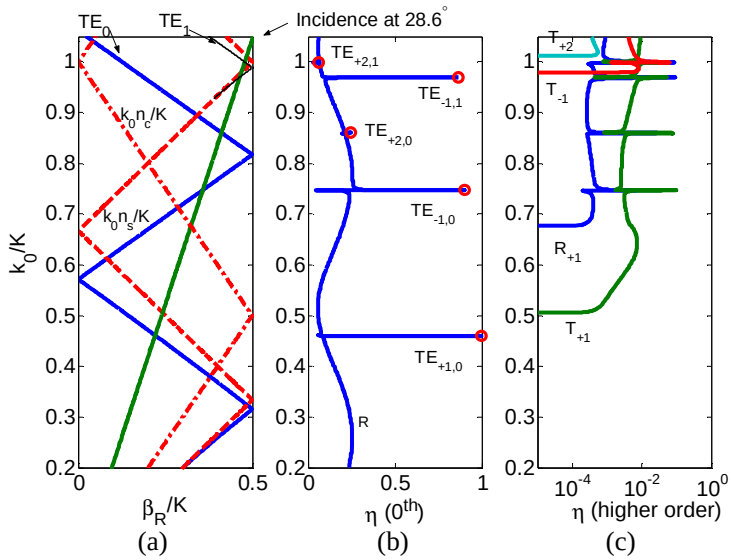

Fig. 12. Dispersion and diffraction picture for an obliquely incident plane wave. The grating has n_h=2.05 and $\Delta\varepsilon$=0.34. (a) Frequency dependence of the real part of the propagation constant and the dispersion curve of the incident wave at θ=28.6°. (b) GMR reflectance of the 0th order labeled with $TE_{m,v}$. (c) Efficiency of higher diffraction orders.

Figures 13(a) -13(c) provide rigorously computed diffraction and dispersion results near the second stop band for the same structure. Figure 13(a) presents the GMR reflection efficiency calculated as function of frequency and angle near normal incidence. This reflectance map in ω-β contains information on both the resonance location and resonance linewidth. The reflectance map shows that the lower edge is the leaky edge indicated by the continuity of the reflectance to the θ=0 point; the upper edge shows no resonance at θ=0 since the profile is symmetric [8]. Figure 13(b) shows a dispersion plot computed with complex frequency with GMR locations noted also. Figure 13(c) provides similar results but with the dispersion computed in real frequency. Comparison of Figs. 13(a)-13(c) shows that the dispersion curves computed with real propagation constant and complex frequency accurately predict the locations at frequencies near the lower band edge.

To excite a resonance with a plane wave incident at angle θ, the phase matching condition

$$k_0 n_c \sin\theta - mK = Re(\beta_\upsilon) \tag{8}$$

is generally used. The results presented in Sec. 4 show that different values of Re(β) pertain to the real ω and complex ω dispersion pictures. The difference between these solutions increases with the modulation $\Delta\varepsilon$. The width of the stop band is ~$2h_2/h_3$ (see Table I), in both cases, is set primarily by h_2 which is proportional to the value of the second Fourier grating harmonic with amplitude γ_2. At the resonant (leaky) edge, the difference in the β-values is due to the leaked wave as demonstrated in Sec. 4. The representation in complex frequency delivers the real propagation constant directly and matches the results from the diffraction computations as demonstrated in Fig 13. Figure 13(c) indicates phase matching to the

#77691 - $15.00 USD Received 1 December 2006; revised 11 January 2007; accepted 12 January 2007
(C) 2007 OSA

deviated part of the curve. It implies that, as an example, for incident wave with θ=0.2°, a resonance should be found at the point marked by '∗' in Fig. 13(c) based on Eq. (8). However, there are no states in the band and this picture is not correct. The phase matching relation that pertains to the correct dispersion plot in Fig. 13(b) is

$$k_0 n_c \sin\theta - mK = \beta_\upsilon \tag{9}$$

where β_ν is real and found by dispersion computations employing complex frequency.

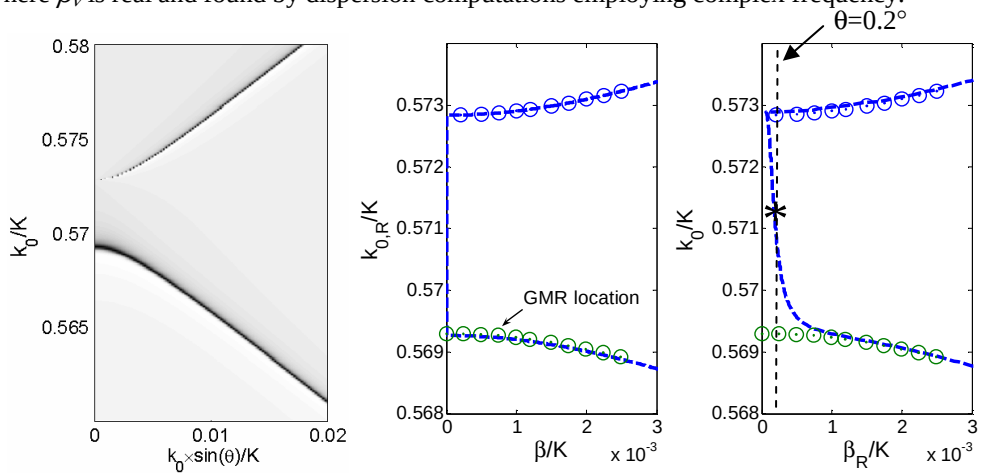

(a) (b) (c)

Fig. 13. GMRs around the second stop band. (a) Diffraction diagram of the GMR reflectance as function of the normalized wave vector k_x/K and frequency k_0/K. (b) Comparison of the β curve (complex frequency) and the locations of GMRs. (c) Comparison of the β_R curve (real frequency) and the locations of GMRs.

A possible interpretation of these results is as follows: The incident wave can phase-match only to the leaky mode and not to the leaked wave since the leaky mode generates the leaked wave. In Sec 4.3, it is shown that the propagation constant computed in real frequency in the band center and at the leaky edge depends on both coefficients h_1 (leak) and h_2 (Bragg). Thus, the leaked wave perturbs the real part of β on which phase-matching proceeds. Assignment of a complex propagation constant to the problem requires spatial Bragg- and radiation decay via Im(β_ν). In contrast, by casting the dispersion computation into the complex frequency domain, the spatial decay mechanisms associated with Bragg reflection and radiation leakage are converted into a single time decay coefficient as described in Sec. 4.3. This renders an unperturbed, real β_ν for input-wave phase matching, avoiding explicit dependence on separate spatial decay mechanisms, and provides consistent results as shown in Fig. 13.

#77691 - $15.00 USD Received 1 December 2006; revised 11 January 2007; accepted 12 January 2007
(C) 2007 OSA

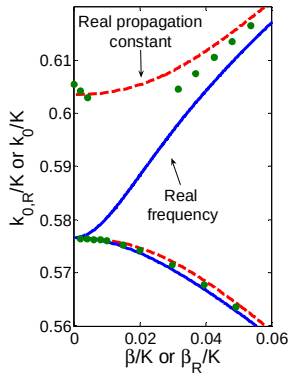

Fig. 14. Comparison of the dispersion curves and the locations of GMRs under strong modulation. The dots represent the resonance locations estimated from diffraction computations for incident angles from 0° to 5°. The structure is the same as that in Fig. 9 with n_h=2.6 and $\Delta\varepsilon$=4.6.

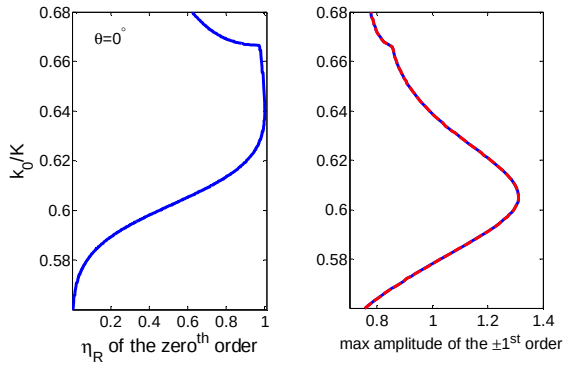

Fig. 15. Diffraction efficiency and the maximum amplitude of the first orders at normal incidence. The structure has n_h=2.6 and $\Delta\varepsilon$=4.6.

With increased modulation, the amplitude of the leaked wave increases substantially such that dispersion curves computed in real frequency may fail to reveal the band structure. Figure 14 shows a Brillouin diagram for a waveguide grating with heavy modulation computed in real and complex frequency whose dispersion characteristics are given in Fig. 9. As in Fig. 13, a clear band gap is shown in complex frequency. Additionally, estimated GMR peak locations are shown agreeing well with the dispersion curve. In Fig. 14, the resonance locations estimated from diffraction computations do not fall precisely on the upper band. This is because accurate resonance locations are difficult to define when the Q factor is very low. Actually, it is infeasible to find the resonance locations based on the diffraction efficiency in this example. Figure 15 shows the zero-order reflectance at normal incidence. Solely based on reflectance, one would expect the resonance to locate at frequency 0.64. Thus, we turn to the locations of the peak amplitudes of the leaky mode excited by the ±1 evanescent diffraction orders (Fig. 15); these appear at frequency 0.605, which is consistent with the dispersion results as shown in Fig. 14. At oblique incidence, the resonance locations at the upper band for certain angles are still difficult to identify even using the near field peaks. This is because the resonance in the lower band, which has narrower linewidth but stronger excited modes, affects the mode amplitude of the resonance at the upper band [4]. With increasing angle, the two resonances separate. Indeed, the upper resonance becomes clearly detectable again for higher incident angles (i.e. θ>5°).

#77691 - $15.00 USD Received 1 December 2006; revised 11 January 2007; accepted 12 January 2007
(C) 2007 OSA

6. Conclusion

In this paper, we have endeavored to formulate and explain the leaky stop bands characteristic of planar periodic waveguides or photonic crystal slabs. These bands differ from Bragg-type stop bands as there exists an out-of-plane radiative energy-coupling channel. We apply a semianalytical model due to Kazarinov and Henry [9] to compute the dispersion curves describing the leaky stop band (second band) and verify its correctness by rigorous band computations. This approximate model provides clear insights into the properties of the leaky stop band on account of analytical expressions obtained that relate band features to the operative physical processes. In particular, it enables comparison of the structure of the bands computed in complex propagation constant, implying spatially decaying leaky modes, with the bands computed in complex frequency, implying temporally decaying modes. It is explicitly shown that coexisting Bragg-coupling and energy-leakage mechanisms perturb the bands in complex propagation constant whereas these mechanisms are decoupled in complex frequency. As a result, the bands in complex frequency are well defined and clear band gap emerges. These conclusions are verified by numerical diffraction computations for both weak and strong grating modulations.

Formulations in terms of complex propagation constant are often used in analysis of the spectral response of periodic waveguides [1]. Band computations in complex propagation constant and complex frequency give similar results when a single mechanism is at work. For example, in the nonleaky stop band, illustrated in Fig. 5, only Bragg reflection is at work and both formulations give equivalent results. Another example is GMR occurrence away from the band. At sufficiently large angle of incidence, there is only out-of-plane radiation induced by the resonant leaky-mode and the solutions again agree as shown in Fig. 13. For very strong modulation, the results of the KH model become inaccurate while retaining qualitative agreement with numerical results. For such cases, as demonstrated in Fig. 14, phase matching to a leaky mode resonance, in or out of band, will accurately proceed via real propagation constant β_ν that is found by dispersion computations employing complex frequency.

Acknowledgment

This material is based, in part, upon work supported by the National Science Foundation under Grant No. ECS-0524383.